Surface treatment of TaN for sub-2 nm, smooth, and conducting atomic layer deposition Ru films \odot

Special Collection: Atomic Layer Deposition (ALD)

Corbin Feit; Udit Kumar ⁽¹⁾; Md. Rafiqul Islam; Luis Tomar; S. Novia Berriel ⁽¹⁾; John T. Gaskins ⁽¹⁾; Patrick E. Hopkins; Sudipta Seal ⁽¹⁾; Parag Banerjee ¹⁰



J. Vac. Sci. Technol. A 42, 032407 (2024) https://doi.org/10.1116/6.0003440





18 May 2024 11:40:40



Cite as: J. Vac. Sci. Technol. A **42**, 032407 (2024); doi: 10.1116/6.0003440 Submitted: 9 January 2024 · Accepted: 7 March 2024 · Published Online: 3 April 2024







Corbin Feit, Udit Kumar, Md. Rafiqul Islam, Luis Tomar, S. Novia Berriel, Dohn T. Gaskins, Datrick E. Hopkins, 4.5 Sudipta Seal, 6 and Parag Banerjee (1.6.7.8,a)

AFFILIATIONS

- Department of Materials Science and Engineering, University of Central Florida, Orlando, Florida 32816
- ²Department of Mechanical and Aerospace Engineering, University of Virginia, Charlottesville, Virginia 22904
- ³Laser Thermal, Charlottesville, Virginia 22902
- Department of Materials Science and Engineering, University of Virginia, Charlottesville, Virginia 22904
- ⁵Department of Physics, University of Virginia, Charlottesville, Virginia 22904
- ⁶Nano Science and Technology Center, University of Central Florida, Orlando, Florida 32816
- Florida Solar Energy Center, University of Central Florida, Orlando, Florida 32816
- ⁸REACT Faculty Cluster, University of Central Florida, Orlando, Florida 32816

Note: This paper is part of the 2024 Special Topic Collection on Atomic Layer Deposition (ALD).

a)Author to whom correspondence should be addressed: parag.banerjee@ucf.edu

ABSTRACT

Atomic layer deposition (ALD) of ruthenium (Ru) is being investigated for next generation interconnects and conducting liners for copper metallization. However, integration of ALD Ru with diffusion barrier refractory metal nitrides, such as tantalum nitride (TaN), continues to be a challenge due to its slow nucleation rates. Here, we demonstrate that an ultraviolet-ozone (UV-O₃) pretreatment of TaN leads to an oxidized surface that favorably alters the deposition characteristics of ALD Ru from islandlike to layer-by-layer growth. The film morphology and properties are evaluated via spectroscopic ellipsometry, atomic force microscopy, electrical sheet resistance measurements, and thermoreflectance. We report a 1.83 nm continuous Ru film with a roughness of 0.19 nm and a sheet resistance of $10.8 \text{ K}\Omega/\square$. The interface chemistry between TaN and Ru is studied by x-ray photoelectron spectroscopy. It is shown that UV-O₃ pretreatment, while oxidizing TaN, enhances Ru film nucleation and limits further oxidation of the underlying TaN during ALD. An oxygen "gettering" mechanism by TaN is proposed to explain reduced oxygen content in the Ru film and higher electrical conductivity compared to Ru deposited on native-TaN. This work provides a simple and effective approach using UV-O₃ pretreatment for obtaining sub-2 nm, smooth, and conducting Ru films on TaN surfaces.

Published under an exclusive license by the AVS. https://doi.org/10.1116/6.0003440

I. INTRODUCTION

The progression of interconnect technologies following Moore's law has met materials and design challenges as the size of interconnects approach sub-10 nm dimensions. Atomic layer deposition (ALD) is the industry standard for thin film deposition of high-k dielectrics. However, depositing ALD based metallic interconnects present challenges due to poor nucleation and growth of the metal film. ²⁻⁴ Current ALD metal chemistries deposit with an islandlike

growth mechanism and result in poor nucleation, especially on industrially relevant tantalum nitride (TaN) diffusion barriers.^{5–8} This growth behavior hinders the coalescence of metal films for thicknesses <10 nm, which can lead to increased surface roughness, the presence of pinholes, and, therefore, enhanced electron scattering and increased line resistance.⁹

Ruthenium (Ru) is a promising alternative to copper interconnects due to its improved electromigration resistance at reduced



line widths. Ru interconnects exclude the need for diffusion barriers compared to copper interconnects. 10-13 Historically, Ru has been used as a seed layer on top of a TaN liner, which aids in the deposition and containment of Cu in the back-end of the line (BEOL) damascene process.^{2,14} Thus, the continued importance of Ru requires processes that enhance nucleation and ensure that film continuity is achieved within the first few nm of film growth.

Ru film deposition using ALD is well established. A review of various Ru ALD chemistries is presented by Austin et al.,5 who note that nucleation delays are a function of precursor and substrate affinity, which vary widely by the ALD process and the target application. This is not surprising as it is known that the surface chemistry of substrates affects the nucleation and growth of ALD films, in general, and affects preliminary reaction rates during film formation. Surface engineering via self-assembled monolayers, small molecule inhibitors, or oxidation/nitridation has shown improvement of ALD nucleation and growth on various surfaces.4

This work investigates the effect of an UV-O3 treatment on TaN surfaces in inducing rapid Ru film nucleation and growth in the sub-2 nm regime. ALD Ru thin films are deposited using Ru-dimethylbutadiene tricarbonyl [Ru(DMBD)(CO)₃] and H₂O (growth rate = 0.1 nm/cy) and have been described in our previous work.²⁰ This molecule has also been recently studied by Schneider et al., who propose a kinetically limited model for the nonselflimiting growth of ALD Ru on SiO₂ surfaces.²¹ We monitor film nucleation by atomic force microscopy (AFM). The Ru thickness (optically transparent for thickness < 15 nm) is measured by spectroscopic ellipsometry (SE). The interface chemistry is probed by x-ray photoelectron spectroscopy (XPS) and water contact angle (WCA) measurements. Electrical and thermal conductance measurements are carried out to detect the onset of film coalescence and continuity. Our results indicate that UV-O3 treatment enhances nucleation and growth of Ru on TaN, resulting in smooth, sub-2 nm, electrically continuous films.

II. EXPERIMENT

Substrates were supplied by Intel® Corporation and consisted of physical vapor deposited 2 nm TaN deposited on 100 nm SiO₂ on Si wafers. The substrates were ultrasonically cleaned with isopropyl alcohol (IPA) and de-ionized water (DIW). For the case where surface oxidation of TaN was required, 5-min exposure to UV-O₃ was conducted by a UV-O₃ cleaner, model E511 (Ossila®). The dominant wavelengths of the UV light are 185 and 254 nm. The lamp power is $20 \,\mu\text{W/cm}^2$.

ALD of Ru was performed using a home-built system coupled with a downstream quadrupole mass spectrometer (QMS).²⁰ Briefly, we use a load-locked, hot-wall, viscous flow reactor, 24 in. long with a 2.5 in. internal diameter. The internal base pressure is 120×10^{-3} Torr as monitored by a Piezo/Pirani Dual Transducer (Model No TRN-910) from A&N Corporation. Purge gas control is obtained using a mass flow controller (Parker, 601 Series) and all the valves are pneumatically controlled ALD Valves (Swagelok®). Ru(DMBD)(CO)₃ (EMD Electronics®) and DIW are used for the metal film deposition onto ~ 2 nm TaN on SiO₂ substrates. The Ru $(DMBD)(CO)_3$ and DIW reactants were kept at 25 ± 1 °C. The ALD furnace temperature was held at 190 °C, and the inlet gas lines were held at 125 °C. Ru(DMBD)(CO)₃ was stored in a stainless steel bubbler and was carried into the reaction chamber by 99.999% pure Ar gas at a rate of 25 standard cubic centimeters per minute (SCCM) for 5 s. Each Ru(DMBD)(CO)₃ pulse was followed by a purge step of 75 SCCM Ar for 25 s. A subsequent vacuum step returned the chamber pressure to baseline before the following reactant DIW was directly introduced from a single outlet ampoule for 1 s. The subsequent purge step followed with 75 SCCM Ar for 25 s then a vacuum step to finish the super cycle. The reaction mechanism is described by Gao et al.²⁰ In brief, a growth per cycle of 0.1 nm/cycle on the planar SiO₂ substrate is reported. Various Ru ALD films of up to 150 cycles were deposited. We note here that the ALD process recipe described here is different from the one reported by Schneider et al.,21 who report a sequential set of micropulses of the Ru(DMBD)(CO)₃. This approach has been shown to lead to a nonself-limiting (i.e., CVD-like) growth behavior of the Ru film. We intentionally avoid such a growth regime as it can lead to nonconformal films inside high aspect ratio structures.

A spectroscopic ellipsometer from J. A. Woollam® M-2000, with a wavelength range from 190 to 1690 nm, was used to measure film growth. The optical models for thin film analysis were built in the COMPLETE EASE software and consisted of an effective medium approximation with a B-spline layer and a void layer to delineate the contributions of islandlike growth behavior. The detailed parameters for each optical model are supplied in supplementary material I.3

Static WCA measurements were taken on an Ossila® E511 and analyzed using Ossila® contact angle software (version 1.1.02). DIW droplets of a volume of $10\,\mu l$ were dropped using a pipet on untreated and UV-O₃ treated TaN film substrates. The surface and interface chemistries of Ru and TaN/TaN-UV-O₃ 8 interface were probed by angle-resolved x-ray photoelectron spectroscopy (XPS) using an ESCALAB-250Xi XPS system from ThermoFisher Scientific®. Experiments were performed at a pressure below $7 \times 10^{-9} \, \text{mbar using Al-K}_{\alpha}$ monochromatic radiation and an operating power of 300 W (15 kV, 20 mA). XPS data analysis and peak deconvolutions were analyzed using the AVANTAGE SURFACE CHEMICAL ANALYSIS software. Binding energies were calibrated using the C 1s peak at 284.6 eV. Atomic force microscopy (AFM) was used to monitor the nucleation and growth behavior of as-deposited Ru ALD films using a Horiba® LabRAM HR Evolution Nano AFM. The tips used for imaging were HQ-NSC15/AL BS (from MikroMasch®). The topology data were collected in the tapping mode. The topology and root-mean-squared (RMS) roughness were evaluated using AIST-NT SPM CONTROL software.

Electrical sheet resistance measurements were carried out in a commercial probe station (Janis® ST500-1-2CX) with Cu-Be probe tips with a $50 \,\mu m$ tip diameter. Indium dots melted on the sample surface served as four electrodes on the four corners of the film in a Van der Pauw configuration. A Keithley® 2400 source meter was used to apply a constant $100 \mu A$ current across adjacent two terminals, while voltage was measured across the other two terminals. Every sample was measured in a series of four measurements by cyclically rotating the current and voltage terminals around the sample. The horizontal and vertical components were averaged and the sheet resistance was obtained using the Van der Pauw formula.²² Electrical resistance was measured at 298 K at ambient, atmospheric pressure.

We use two different noncontact, optical pump-probe techniques to measure the thermal conductance of the Ru films-time domain thermoreflectance (TDTR) and steady-state thermoreflectance (SSTR). In doing so, we also demonstrate that these techniques can provide a novel noncontact method to detect changes in Ru nucleation, film coalescence, and subsequent growth. The common principle between both thermoreflectance techniques is that both rely on laser-based pump-probe methods, in which one laser source is used to provide a localized and modulated heating event to the sample, causing perturbative temperature fluctuations on the sample surface, while a secondary laser source probes the change in reflectivity due to this pump thermal perturbation. This change in probe beam reflectivity is then related to the temperature change on the sample surface, which is in turn related to the thermal resistance giving rise to the thermal gradient induced by the pump heater. This thermal gradient is impacted by the Ru films, and we determine this thermal resistance based on various thermal models rooted in the cylindrical heat equation. The TDTR measurements are based around a home-built system centered on a subpicosecond Spectra Physics Tsunami with a central wavelength of 808 nm. The SSTR measurements are conducted with the commercial SSTR-F system from Laser Thermal. Details of both techniques and systems are provided in supplemental material II.3

III. RESULTS AND DISCUSSION

A. Water contact angle

Static WCA measurements are performed to understand the effect of UV-O₃ treatment on the surface energy of TaN. Figure 1 shows the effect of UV-ozone pretreatment on the TaN hydrophilicity. The as-deposited TaN exhibits a WCA of $68.0 \pm 0.4^{\circ}$. Upon exposure to UV-ozone for varying times, the WCA decreases to $36.6 \pm 3.4^{\circ}$, $13.3 \pm 3.5^{\circ}$, and $5.5 \pm 3.2^{\circ}$ after 1, 3, and 5 min, respectively. The increase in hydrophilicity is attributed to surface oxidation of the TaN to TaON, which is discussed in greater detail below.

B. Spectroscopic ellipsometry

The growth of <5 nm Ru ALD films is inherently challenging due to the islandlike growth behavior associated with the Ru (DMBD)(CO)₃ precursor. The growth behavior of Ru ALD on TaN substrates is studied by *ex situ* ellipsometry and shown in Fig. 2. The data are collectively summarized in Table I. The growth per cycle in the linear regime for Ru ALD on native-TaN is measured to be 0.08 nm/cy. This value is consistent with the 0.1 nm/cy reported in the literature for Ru(DMBD)(CO)₃ with H₂O.²⁰

We use a convention where the incubation cycle "c" is measured as [Eq. (1)]

$$c = 100 - \frac{t}{g},\tag{1}$$

where t is the final thickness (nm) at 100 cycles and g is the growth per cycle (nm/cy).¹⁷ As a result, a nucleation delay of ~16 cycles is estimated on the native-TaN substrate. On the other hand, the UV-O₃ treated TaN data results in an estimated nucleation delay of ~2 cycles *only*, which signifies enhanced nucleation.

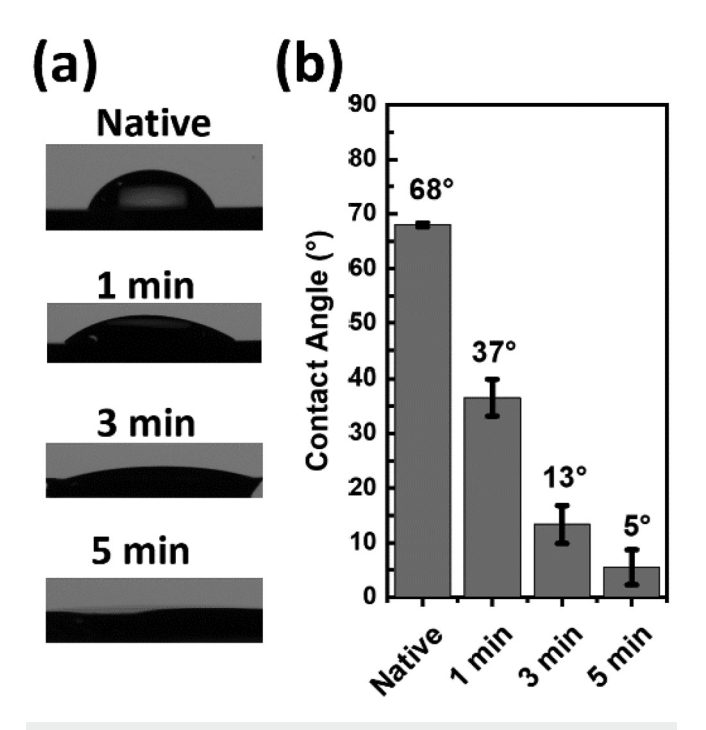


FIG. 1. (a) Images of water droplets on UV-O $_3$ treated TaN, as a function of exposure time. (b) Water contact angles on TaN with an increase in UV-O $_3$ exposure time.

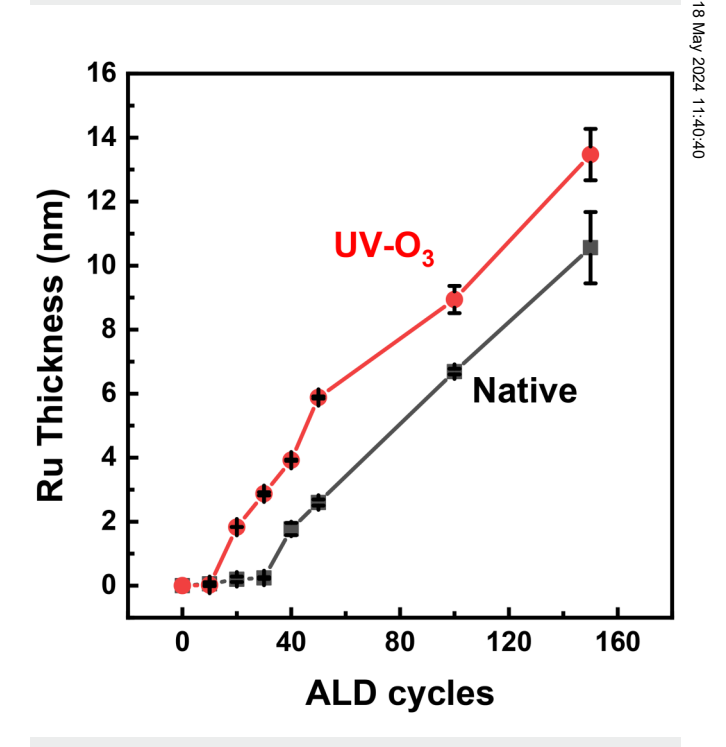


FIG. 2. Spectroscopic ellipsometry data showing Ru film thickness on native-TaN and UV-O₃-TaN, as a function of ALD cycles.

 TABLE I. Summary of the film thickness calculated by spectroscopic ellipsometry.

ALD number of cycles	Ru thickness on native-TaN (nm)	Ru thickness on UV-O ₃ -TaN (nm)
10 20	0.06 ± 0.10 0.20 ± 0.10	0.02 ± 0.03 1.80 ± 0.03
30 40	0.24 ± 0.02 1.80 ± 0.20	2.90 ± 0.05 3.90 ± 0.02
50	2.60 ± 0.10	5.90 ± 0.03
100 150	6.70 ± 0.10 10.60 ± 0.10	8.90 ± 0.40 13.50 ± 0.80

These results are further exemplified when comparing thickness at 150 cycles for both sets of samples; the native-TaN results in a Ru film of 10.6 ± 1.1 nm, while the UV-O₃ sample has a Ru film of 13.5 ± 0.8 nm.

C. Atomic force microscopy

To further confirm the growth behavior reported by SE above, the surfaces of the Ru films are analyzed by AFM. Figure 3(a) shows the progression of Ru growth on native-TaN and on UV-O₃-TaN. The nucleation delay observed on native-TaN is correlated with islandlike growth that ultimately leads to enhanced surface roughness at the point of coalescence. 23,24 The individual grains become increasingly discernable with increasing cycles. The results from AFM scans can be quantified further. The Ru films grown on native-TaN exhibit a high degree of root-mean-squared (RMS) roughness compared to Ru films on UV-O3-TaN. This is shown in surface roughness graphs in Fig. 3(b). This growth characteristic is associated with (1) the formation of nuclei, (2) nuclei coalescence at peak RMS roughness, and (3) a gradual decrease in RMS roughness as nuclei merge to form a continuous Ru film.²⁴ We see that nuclei coalescence of Ru on native-TaN occurs at ~75 cycles.

The growth behavior of Ru on UV-O₃-TaN does not lead to a peak increase in roughness with increasing ALD cycles, indicating quick nucleation followed by layer-by-layer growth of the Ru film. The RMS roughness of Ru on UV-O₃-TaN remains consistently lower than the Ru on native-TaN. For example, the RMS roughness for 150 cycles of Ru on native-TaN is much higher $(0.60\pm0.10~\text{nm})$ compared to 150 cycles of Ru ALD on UV-O₃-TaN $(0.25\pm0.01~\text{nm})$. Thus, AFM data demonstrates improved Ru film quality on the UV-O₃-TaN.

D. Electrical conductivity

When metallic films proceed via island growth, a high number of ALD cycles are required before a conductive pathway forms. Alternatively, in a layer-by-layer growth mechanism, a conductive pathway is established at the onset of the ALD process. This effect is clearly observable when measuring the sheet resistance of the Ru films as a function of ALD cycle numbers, as shown in Fig. 4. The native-TaN substrate shows $269 \pm 42 \text{ M}\Omega/\square$ with a slight increase in resistance after UV-O₃-TaN with 389 ± 49 M Ω / \square (i.e., at 0 ALD cycles). This is expected as the surface of UV-O₃-TaN is oxidized. The high resistance is maintained for the native-TaN until 50 ALD cycles (thickness = 2.6 ± 0.1 nm) when a conductive path is formed resulting in a sheet resistance of $\sim 1.0 \pm 0.01 \text{ K}\Omega/\Box$. We note that the RMS roughness results from AFM data show ~ 75 ALD cycles are required to achieve nuclei coalescence. This discrepancy between AFM and electrical data suggests that despite electrical continuity at 50 cycles, nanoscopic discontinuities may exist in the ties, a conductive pathway may exist. After 150 cycles Ru ALD $\stackrel{\bigcirc}{\approx}$ (thickness = 10.6 ± 1.1 nm) on pative TaN 6-11 be assumed with a sheet resistance of $83.9 \pm 0.01 \Omega/\Box$.

On the other hand, the UV-O₃-TaN requires only 20 cycles of $\frac{5}{8}$ Ru ALD (thickness = 1.83 ± 0.03 nm) to form a conductive pathway. The sheet resistance is 10.8 ± 0.0001 K Ω/\Box . Due to the 1.83 nm thickness of Ru, electron scattering via defect, grain boundary,

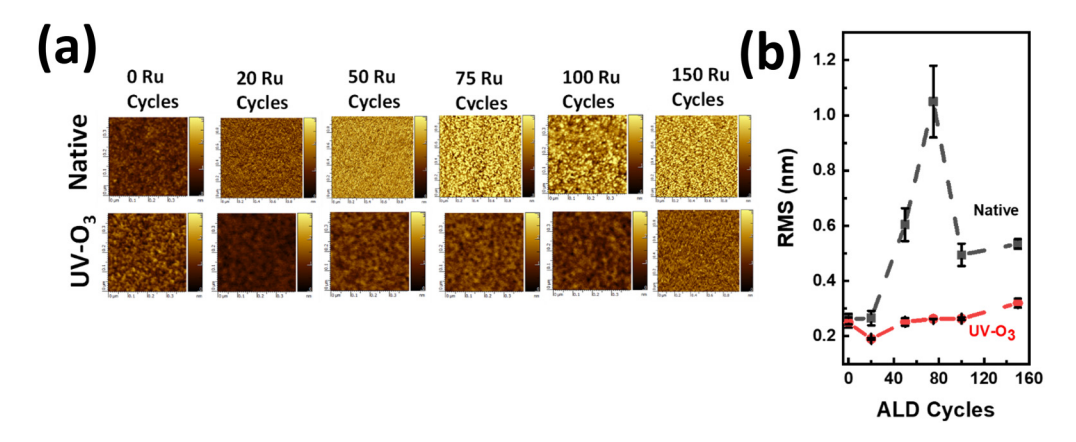


FIG. 3. (a) Atomic force microscopy images of Ru films on native and UV-O₃-TaN. The scan areas were kept constant $(1.0 \, \mu \text{m}^2)$ across samples with $0.4 \, \mu \text{m}^2$ shown to improve observation of grains. The scale bar for height varies from 0.0 to 3.0 nm and is also kept constant across all scans. (b) Calculated root mean square roughness of the respective Ru films (sample size for each measurement, n = 3).

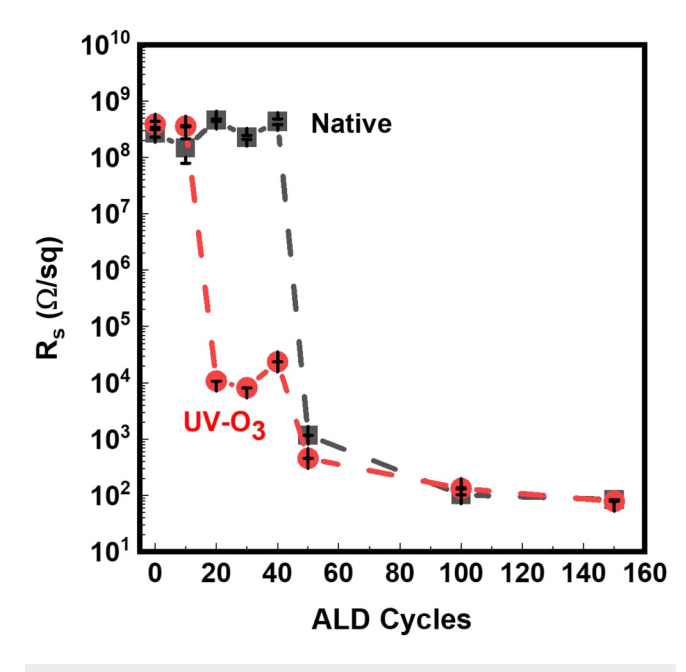


FIG. 4. Semi-log plot of sheet resistance of Ru ALD films on native-TaN and UV-O₃-TaN, demonstrating the number of ALD cycles required to establish electrical continuity.

and surface scattering, causes the sheet resistance to be relatively high. 10,12,13 From 50 cycles to 150 cycles of Ru ALD on UV-O₃-TaN, the sheet resistance drops from 454 ± 2 to $78 \pm 0.1 \Omega/\square$. These results demonstrate that UV-O₃ treatment of TaN enhances the Ru ALD growth enabling 20 ALD cycles (thickness = 1.83 ± 0.03 nm) to demonstrate conductive behavior. Without the surface treatment, 50 cycles of Ru ALD (thickness = 5.90 ± 0.03 nm, i.e., $3 \times$ thicker) is required to achieve similar conductivity.

E. Thermal conductivity

Noncontact based pump-probe measurements are used to measure the effects of nucleation and coalescence on film thermal conductivity. We show the changes in thermal resistances of the various Ru films as measured with SSTR as a function of sheet resistance and the Ru film thickness in Figs. 5(a) and 5(b), respectively. The details of the SSTR analysis are discussed in supplementary material II³³ along with the corroborating TDTR measurements. Prior to SSTR and TDTR measurements, a thin (~80 nm) Al transducer is deposited on the sample surface for consistent opto-thermal transduction of the pump and probe energies among all samples. The thermal resistance measured with SSTR is indicative of the resistance of the Ru/TaN/SiO₂ multilayer stack along with corresponding thermal boundary resistances at the Al/Ru and SiO₂/Si interfaces. We discuss the assumptions involved with extracting the thermal resistance of the Ru/TaN film separately from the thermal resistance of the SiO₂ and corresponding interfaces in supplementary material II.33

Observational conclusions show that the thermal resistance of the films increases with (a) decreasing sheet resistance, i.e., increasing film thickness. The increase in thermal resistance with increasing thickness is consistent with diffusive thermal transport, in that adding more material to the interface will increase the resistance of (proportional to the thickness of the film). While the increase in thermal resistance with decreasing sheet resistance may at first seem counterintuitive, this is consistent with diffusive thermal

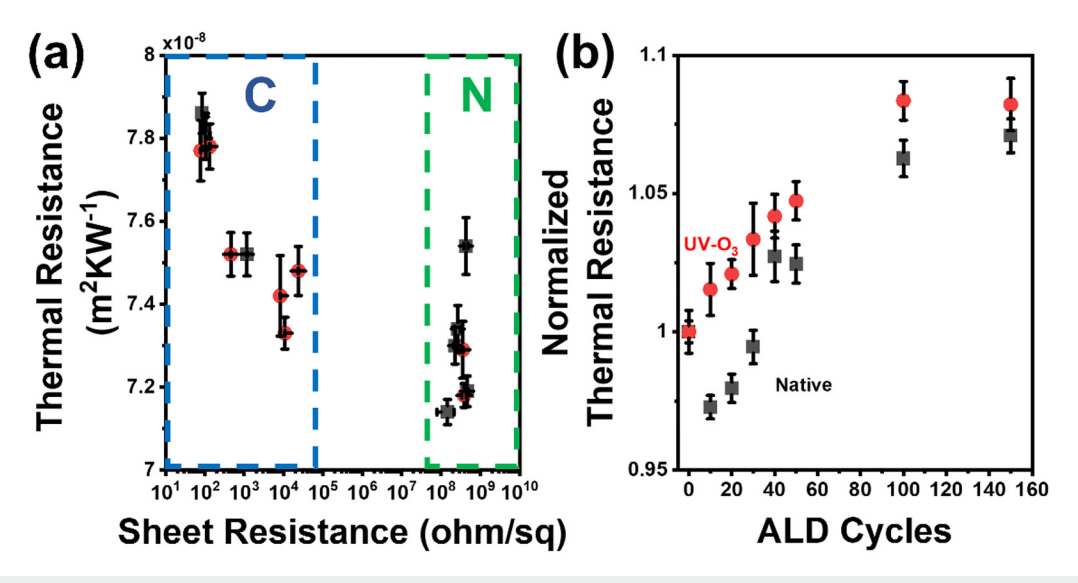


FIG. 5. SSTR measurements: (a) Thermal resistance across Ru/TaN/SiO2 as a function of Ru sheet resistance. "C" and "N" regions represent the coalescence and nucleation regions, respectively, for native-TaN. Square symbols are native-TaN. Circular symbols are UV-O₃-TaN. (b) The normalized thermal resistance as a function of the Ru film thickness. Thermal resistance increases with the Ru film thickness because electrons scatter more elastically and diffuse further.



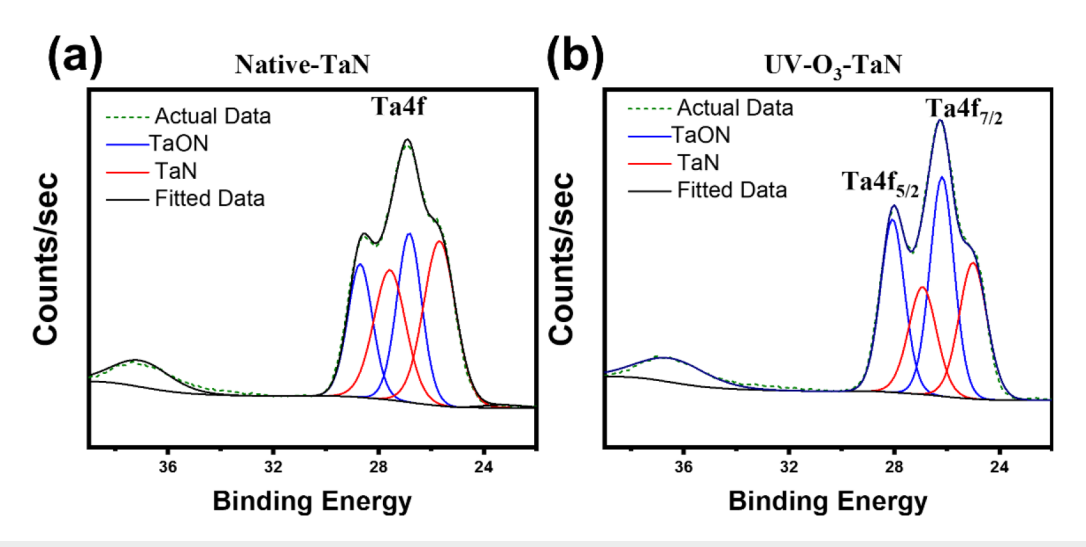


FIG. 6. Ta 4f spectra (a) on native-TaN and (b) on UV-O₃ treated TaN.

transport, demonstrating SSTR (and thermal resistance measurements, in general) as a unique noncontact method to detect film coalescence and growth.

Figure 5(a) shows the thermal resistance (m²/KW) of Ru films as a function of sheet resistance. Film continuity is required to offer a reasonable change in thermal resistance. The nucleation and coalescence regions are outlined in Fig. 5(a) as "N" and "C," respectively. 0-40 ALD cycles of Ru on native-TaN populate the nucleation region, where sheet resistance exceeds $10^8 \Omega/\Box$ and thermal resistance varies from $\sim 7.2-7.6 \times 10^{-8} \text{ m}^2/\text{KW}$. ALD cycles from 50 to 150 on native-TaN populate the coalescence "C" region, where sheet resistance dramatically reduces to $10^2-10^3 \Omega/\Box$ and thermal resistance varies from ~ 7.5 to 7.9×10^{-8} m²/KW. Alternatively, 0-10 ALD cycles of Ru on UV-O₃-TaN populate the nucleation region, where sheet resistance exceeds $10^8 \Omega/\Box$ and thermal resistance varies from ~ 7.1 to 7.4×10^{-8} m²/KW. 30–150 ALD cycles of Ru on UV-O₃-TaN populate the coalescence region, where sheet resistance reduces to $10^2-10^4 \Omega/\Box$ and thermal resistance varies from ~ 7.4 to 7.9×10^{-8} m²/KW. It can be concluded that the thermal boundary resistance and sheet resistance of Ru on native-TaN and UV-O₃-TaN do not significantly change until a critical number of ALD cycles is reached that leads to film coalescence and continuity, consistent with Fig. 4.

To differentiate Ru growth onset between the native-TaN and UV-O₃-TaN, we normalize SSTR resistances by the resistance at 0 cycles Ru ALD, i.e., substrate only. Figure 5(b) shows initially, the thermal resistance decreases for Ru ALD on native-TaN. This may be attributed to surface oxidation during the island growth of Ru, which will be discussed in Sec. III F. Ru films on native-TaN do not exhibit an appreciable increase in thermal resistance, compared to native-TaN, before 30 ALD cycles (0.24 ± 0.02 nm). However, the thermal resistance increases abruptly at 40-50 ALD cycles (1.8-2.6 nm) indicating nuclei coalescence, consistent with the ellipsometry, AFM, and sheet resistance measurements, described earlier. On the other hand, the normalized thermal resistance of

the Ru film on UV-O₃-TaN shows a distinct increase in thermal resistance after 20 cycles (thickness = 1.83 ± 0.03 nm) indicating that a higher areal fraction of the UV-O₃-TaN substrate is covered with the Ru film compared to 20 ALD cycles on native-TaN. The change in thermal resistance after 150 cycles of Ru (thickness on native-TaN = 10.6 ± 1.1 nm and on UV-O₃-TaN = 13.47 ± 0.80 nm) is leveled off, indicating a complete surface coverage and the onset of bulk Ru thermal properties. The SSTR results are consistent with diffusive thermal transport theory and also with our TDTR measurements described in supplementary material II.²

F. X-ray photoelectron spectroscopy

XPS is used to investigate the role of the native-TaN and UV-O₃-TaN surface chemistries on Ru ALD. First, we evaluate the TaN surfaces without any overlying Ru film. As is to be expected, UV-O₃ treatment should oxidize the surface and is expected to increase TaON content. Indeed, the Ta 4f spectra on native-TaN [Fig. 6(a)] and UV-O₃-TaN [Fig. 6(b)] without Ru ALD show an increase in the Ta associated with the oxynitride phase upon UV-O₃ treatment. Here, the Ta peaks $(4f_{7/2}$ and $4f_{5/2})$ associated with the nitride are centered at 25.0 and 26.9 eV, while the Ta associated with the TaON is centered at 26.1 and 28.0 eV.28 The ratio of

TABLE II. Ru/RuO2 and TaN/TaON ratio estimated from the area under the curve in Ru3p (ΣRu⁰/σRuO₂) and Ta4f (ΣTaN/ΣTaON) XPS spectra of Ru thin films deposited on TaN.

Sample	Ru/RuO ₂	TaN/TaON
TaN (control)	_	1.25
UV-O ₃ -TaN	_	0.72
TaN + 20 cy Ru ALD	1.26	0.17
UV-O ₃ -TaN + 20 cy Ru ALD	1.97	0.40

the cumulative area under the peaks denoted as $\Sigma TaN/\Sigma TaON$ can be obtained as 1.25 and 0.72, respectively (as shown in Table II). This result is consistent with the static WCA measurements in Fig. 1 and indicates an N-rich native-TaN (less hydrophilic) and an O-rich UV-O₃-TaN surface (more hydrophilic), which is expected based on previous reports of the UV-O₃ treated surface.

Next, we evaluate the interaction of ALD Ru on the two surfaces. For this, a 20 cycle ALD Ru is deposited to ensure that the Ru thickness is low enough for the photoelectrons to escape the Ru layer as well as the underlying TaN substrate (\sim 3 nm). Ru 3p spectrum on native-TaN with 20 Ru cycles is shown in Fig. 7(a). Peaks corresponding to Ru metal (3p_{3/2} and 3p_{1/2}) centered at 462.8 and 484.4 eV, and peaks corresponding to RuO₂ centered at 466.5 and 487.2 eV are observed. Ru signal from the film deposited on UV-O₃-TaN is shown in Fig. 7(b). Similar observations are noted with peaks corresponding to Ru metal centered at 462.0 and 484.0 eV and peaks corresponding to RuO₂ centered at 466.1 and 486.8 eV. These signals can be quantified with the ratio Σ RuO₂ which provide an estimation of the oxidized state of the

ALD Ru film. The values are tabulated in Table II. The $\Sigma Ru^0/\Sigma RuO_2$ ratio is 1.26 and 1.97 for Ru ALD on native-TaN and UV-O₃-TaN, respectively. This result signifies increased metallic Ru content on UV-O₃-TaN compared to native-TaN.

The oxidation state of the underlying substrate, post-Ru ALD is also measured. The Ta 4f spectra for 20 Ru cycles on native-TaN and UV-O₃-TaN are shown in Figs. 7(c) and 7(d), respectively. The Ta 4f spectrum for native-TaN with 20 Ru cycles shows peaks corresponding to TaN and centered at 25.0 and 26.9 eV. In addition, peaks corresponding to TaON are centered at 26.1 and 28.0 eV. Now, the estimated ratio of Σ TaN/ Σ TaON is 0.17 for native-TaN and 0.40 for UV-O₃ treated TaN. These data are presented in Table II. Thus, the native-TaN surface undergoes significant oxidation during the Ru ALD process (Σ TaN/ Σ TaON changes from 1.25 to 0.17). In contrast, the UV-O₃-TaN surface undergoes oxidation upon Ru deposition, but the oxidation is not as severe as the native-TaN surface (Σ TaN/ Σ TaON decreases from 0.72 to 0.40).

Collectively, the data from XPS help us understand the Ru interaction chemistry with the two TaN surfaces in this study.

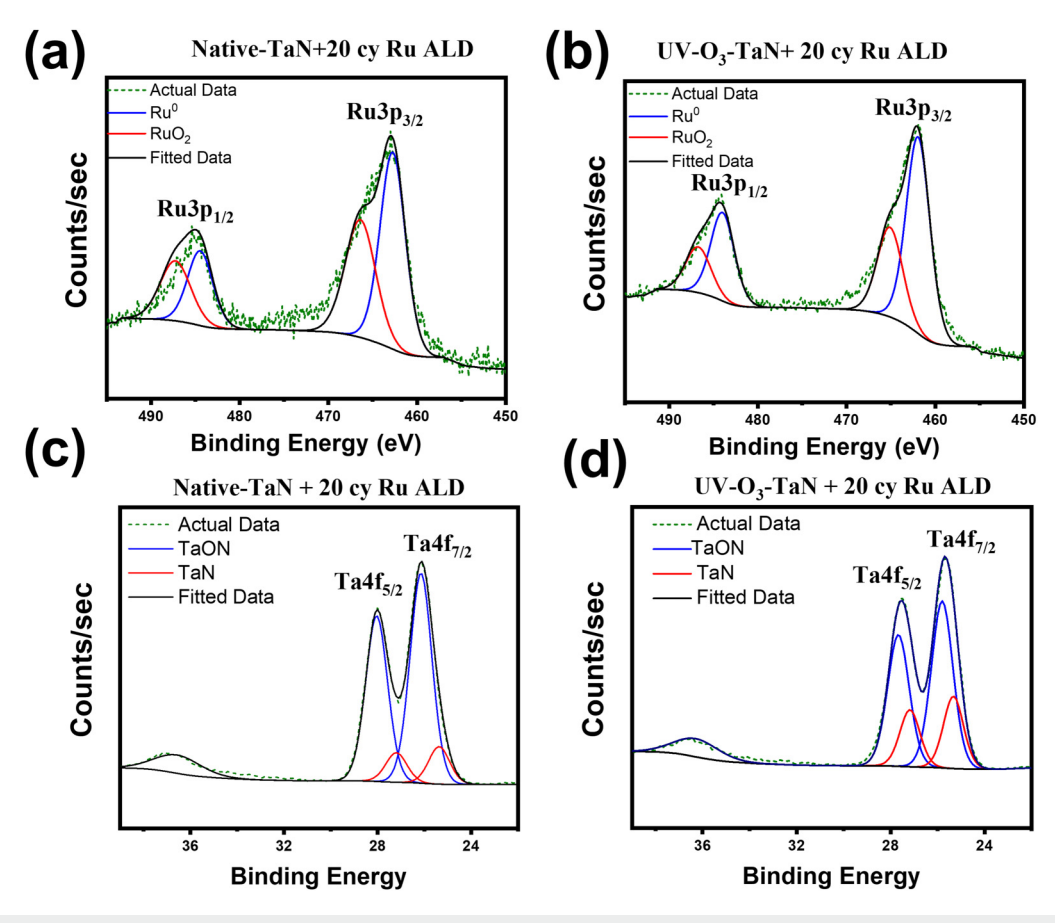


FIG. 7. XPS analysis of Ru metal ALD on the TaN-Si substrate with no surface treatment (native) and UV-O₃-TaN surface treatment. (a) and (b) show Ru 3p spectra for native and UV-O₃ treated TaN, respectively. Peaks corresponding to Ru (metal) and RuO₂ were observed in both samples. (c) and (d) show Ta 4f spectra for native and UV-O₃ treated TaN after Ru ALD, respectively. Peaks corresponding to TaN and TaON were observed in both samples, and a plasmon loss feature peak was also noted.

The nucleation and growth characteristics of the Ru ALD film on the native-TaN surface result in the exposure of TaN to the H2O half-cycles for a longer period of time (~16 cycles based on the incubation formula). Thus, native-TaN undergoes oxidation during the Ru ALD as a result of H₂O exposure. Once a conformal Ru film is formed, further H2O exposure to the underlying TaN is avoided and TaN oxidation terminates. On the other hand, the UV-O₃-TaN surface initiates a quick Ru film nucleation and coalescence leading to the formation of a continuous film within the first few cycles (~2 cycles based on incubation formula). This prevents continued oxidation of the underlying TaN and explains the observed trends in the oxidation of TaN before and after Ru deposition.

The XPS data also suggest that there is oxygen content in the 20 ALD cycle Ru films. However, the Ru deposited on UV-O₃-TaN is more metallic ($\Sigma Ru^0/\Sigma RuO_2 = 1.97$) than the Ru grown on native-TaN ($\Sigma Ru^0/\Sigma RuO_2 = 1.26$). These data are consistent with the superior electrical conductivity of Ru on UV-O3-TaN at 20 ALD cycle. We, thus, hypothesize that, while the ALD process chemistry is the same across both sets of samples, the reason for the improved metallicity of the Ru on UV-O₃-TaN is an "O-gettering effect" by the underlying TaN which removes the O from the Ru film making it more conducting. The ability to effectively get O depends on the degree of oxidation of the TaN. A heavily oxidized TaN-one that results from native-TaN during Ru deposition-will have a lower driving force for the removal of O from the overlying Ru film, as compared to UV-O₃-TaN which remains protected during the Ru ALD process.

IV. SUMMARY AND CONCLUSIONS

Current Ru ALD processes proceed through islandlike growth as a result of poor nucleation on surfaces, especially on TaN barrier films, which are of relevance to the copper damascene based metallization technology. The Ru growth behavior hinders coalescence in the <10 nm regime leading to electrically discontinuous films with poor diffusion characteristics. On the other hand, depositing Ru films past coalescence (>10 nm) leads to increased film surface roughness and lower available volume for copper deposition inside nano trenches of a damascene structure. A potential approach for improved Ru nucleation and growth can be achieved by rationally engineering TaN surfaces that favorably initiate the ALD reactions.

In this work, native-TaN surfaces are shown to induce a nucleation delay (~16 cycles) and roughness (>0.5 nm) of Ru ALD films. However, a UV-O₃ pretreatment on native-TaN can lead to immediate nucleation of the Ru film (~2 cycles) and a marked decrease in Ru film roughness (~0.19 nm) is demonstrated. The role of TaN oxidation on nucleation and growth is understood using water contact angle measurements that show increased hydrophilicity of the TaN surface upon UV-O₃ pretreatment. Evidence of enhanced nucleation is provided via spectroscopic ellipsometry, atomic force microscopy, electrical sheet resistance, and steady-state thermoreflectance measurements of the Ru on native-TaN and UV-O₃-TaN films. The enhanced nucleation and growth of Ru ALD on UV-O3 treated TaN is attributed to increased surface reactivity of Ru precursor-Ru(DMDB)(CO)3 on oxidized TaN. XPS analysis of the films indicates a TaN induced

"O-gettering" mechanism that removes O from the overlying Ru film. UV-O₃ pretreatment enhances the nucleation and growth of Ru films on TaN surfaces resulting in ultra-smooth and electrically conducting 1.83 nm Ru films. This work demonstrates a simple and effective surface engineering approach for the deposition of ultrathin Ru ALD films that can serve as a replacement material for copper interconnects or as ultrathin barrier liners in the next generation of interconnect technologies.

ACKNOWLEDGMENTS

C.F. and P.B. wish to thank Semiconductor Research Corporation for their support of this work under Grant No. 3026.001. C.F. was supported by National Science Foundation (NSF) Grant No. 1908167. L.T. was supported by NSF (Grant No. 2121953). The XPS work was supported via NSF MRI Award, Grant No. 1726636. Md.R.I. and P.E.H. were supported from the Semiconductor Research Corporation, Grant No. 2021-NM-3047, and the NSF, Grant No. 2318576. Samples from Dr. Scott Clendenning from Intel Corporation® are acknowledged. Precursor support of EMD Electronics® is acknowledged.

AUTHOR DECLARATIONS

Conflict of Interest

The authors have no conflicts to disclose.

Author Contributions

Author Contributions

Corbin Feit: Conceptualization (equal); Data curation (equal);
Formal analysis (equal); Investigation (equal); Methodology & (equal); Validation (equal); Visualization (equal); Writing – original draft (equal); Writing – review & editing (equal). **Udit Kumar:** Data curation (equal); Formal analysis (equal); Investigation (equal); Methodology (equal); Writing - original draft (equal). Md. Rafiqul Islam: Data curation (equal); Formal analysis (equal); Investigation (equal); Methodology (equal); Writing - original draft (equal). Luis Tomar: Formal analysis (equal); Investigation (equal); Methodology (equal). S. Novia Berriel: Data curation (equal); Formal analysis (equal); Investigation (equal); Methodology (equal). John T. Gaskins: Resources (equal); Software (equal); Supervision (equal); Writing - review & editing (equal). Patrick E. Hopkins: Funding acquisition (equal); Project administration (equal); Resources (equal); Software (equal); Supervision (equal); Writing - review & editing (equal). Sudipta Seal: Funding acquisition (equal); Project administration (equal); Resources (equal); Software (equal); Supervision (equal); Writing review & editing (equal). Parag Banerjee: Conceptualization (equal); Data curation (equal); Investigation (equal); Methodology (equal); Project administration (equal); Supervision (equal); Validation (equal); Visualization (equal); Writing - original draft (equal); Writing - review & editing (equal).

DATA AVAILABILITY

The data that support the findings of this study are available from the corresponding author upon reasonable request.

REFERENCES

- ¹C. Arenas, G. Herrera, E. Muñoz, and R. C. Munoz, Mater. Res. Express 8, 015026 (2021).
- ²C. C. Yang, S. Cohen, T. Shaw, P. C. Wang, T. Nogami, and D. Edelstein, IEEE Electron Device Lett. 31, 722 (2010).
- ³T. Nogami *et al.*, "High reliability 32 nm Cu/ULK BEOL based on PVD CuMn seed, and its extendibility," in *2010 International Electron Devices Meeting*, San Francisco, CA, 6–8 December, 2010 (IEEE, New York, 2010).
- ⁴C. De Paula, N. E. Richey, L. Zeng, and S. F. Bent, Chem. Mater. 32, 315 (2020).
- ⁵D. Z. Austin, M. A. Jenkins, D. Allman, S. Hose, D. Price, C. L. Dezelah, and J. F. Conley, Chem. Mater. **29**, 1107 (2017).
- ⁶Q. Xie et al., Thin Solid Films 517, 4689 (2009).
- ⁷B. H. Choi, Y. H. Lim, J. H. Lee, Y. B. Kim, H.-N. Lee, and H. K. Lee, Microelectron. Eng. **87**, 1391 (2010).
- ⁸H. Kim, Surf. Coat. Technol. 200, 3104 (2006).
- ⁹Z. Zhang and M. G. Lagally, Science **276**, 377 (1997).
- ¹⁰D. Gall, J. Appl. Phys. **119**, 085101 (2016).
- ¹¹D. Gall, A. Jog, and T. Zhou, "Narrow interconnects: The most conductive metals," in *2020 IEEE International Electron Devices Meeting (IEDM)*, San Francisco, CA, 2020 (IEEE, New York, 2020), pp. 32.3.1–32.3.4.
- 12 T. Zhou and D. Gall, Phys. Rev. B 97, 165406 (2018).
- ¹³D. Gall, J. Appl. Phys. **127**, 050901 (2020).
- ¹⁴O.-K. Kwon, J.-H. Kim, H.-S. Park, and S.-W. Kang, J. Electrochem. Soc. 151, G109 (2004).
- ¹⁵S. M. George, A. W. Ott, and J. W. Klaus, J. Phys. Chem. **100**, 13121 (1996).
- ¹⁶Y. H. Park, M. H. Kim, S. B. Kim, H. J. Jung, K. Chae, Y. H. Ahn, J.-Y. Park, F. Rotermund, and S. W. Lee, Chem. Mater. 28, 7268 (2016).
- ¹⁷C. Feit, J. Sosa, A. Kostogiannes, M. Chazot, N. G. Rudawski, T. Jurca, K. A. Richardson, and P. Banerjee, J. Vac. Sci. Technol. A 40, 052402 (2022).

- ¹⁸J. Yarbrough, A. B. Shearer, and S. F. Bent, J. Vac. Sci. Technol. A **39**, 021002 (2021).
- ¹⁹J. Lee, J. M. Lee, H. Oh, C. Kim, J. Kim, D. H. Kim, B. Shong, T. J. Park, and W. H. Kim, Adv. Funct. Mater. **31**, 2102556 (2021).
- ²⁰Z. Gao, D. Le, A. Khaniya, C. L. Dezelah, J. Woodruff, R. K. Kanjolia, W. E. Kaden, T. S. Rahman, and P. Banerjee, Chem. Mater. 31, 1304 (2019).
- ²¹J. R. Schneider, C. de Paula, J. Lewis, J. Woodruff, J. A. Raiford, and S. F. Bent, Small 18, e2105513 (2022).
- ²²D. K. Schroder, Semiconductor Material and Device Characterization (Wiley, New York, 2015).
- ²³R. L. Puurunen and W. Vandervorst, J. Appl. Phys. **96**, 7686 (2004).
- ²⁴Z. Gao, M. M. R. Hussain, D. De Ceglia, M. A. Vincenti, A. Sarangan, I. Agha, M. Scalora, J. W. Haus, and P. Banerjee, Appl. Phys. Lett. 111, 161601 (2017).
- ²⁵P. E. Hopkins, P. M. Norris, R. J. Stevens, T. E. Beechem, and S. Graham, J. Heat Trans. 130, 062402 (2008).
- ²⁶A. Giri and P. E. Hopkins, Adv. Funct. Mater. **30**, 1903857 (2020).
- ²⁷E. Swartz and R. Pohl, Appl. Phys. Lett. **51**, 2200 (1987).
- ²⁸D. Cristea, L. Cunha, C. Gabor, I. Ghiuta, C. Croitoru, A. Marin, L. Velicu, A. Besleaga, and B. Vasile, Nanomaterials 9, 476 (2019).
- ²⁹J. R. Vig, J. Vac. Sci. Technol. A 3, 1027 (1985).
- 30 J. Hrbek, D. G. van Campen, and I. J. Malik, J. Vac. Sci. Technol. A 13, 1409 (1995).
- ³¹Y. Li, Q. Zhang, N. Zhang, L. Zhu, J. Zheng, and B. H. Chen, Int. J. Hydrogen Energy 38, 13360 (2013).
- ³²J. V. Rojas, M. Toro-Gonzalez, M. C. Molina-Higgins, and C. E. Castano, Mater. Sci. Eng. B **205**, 28 (2016).
- 33See the supplementary material for the spectroscopic ellipsometry model for Ru on TaN and experimental and modeling details on time domain thermoreflectance (TDTR) and steady-state thermoreflectance (SSTR).